nature COMMUNICATIONS

ARTICLE

DOI: 10.1038/s41467-017-00558-9 OPEN

# Controlling selectivities in $CO_2$ reduction through mechanistic understanding

Xiang Wang[1], Hui Shi[1] & János Szanyi[1]

Catalytic $CO_2$ conversion to energy carriers and intermediates is of utmost importance to energy and environmental goals. However, the lack of fundamental understanding of the reaction mechanism renders designing a selective catalyst inefficient. Here we show the correlation between the kinetics of product formation and those of surface species conversion during $CO_2$ reduction over $Pd/Al_2O_3$ catalysts. The *operando* transmission FTIR/SSITKA (Fourier transform infrared spectroscopy/steady-state isotopic transient kinetic analysis) experiments demonstrates that the rate-determining step for CO formation is the conversion of adsorbed formate, whereas that for $CH_4$ formation is the hydrogenation of adsorbed carbonyl. The balance of the hydrogenation kinetics between adsorbed formates and carbonyls governs the selectivities to $CH_4$ and CO. We apply this knowledge to the catalyst design and achieve high selectivities to desired products.

[1] Institute for Integrated Catalysis, Pacific Northwest National Laboratory, Richland, WA 99352, USA. Correspondence and requests for materials should be addressed to J.S. (email: janos.szanyi@pnnl.gov)

Heterogeneous catalytic $CO_2$ reduction has been attracting great attention, because it not only mitigates the risks associated with increasing $CO_2$ concentration in the atmosphere but also offers a variety of pathways for producing fuels and industrial chemicals[1, 2]. Under atmospheric pressure, methanation and reverse water gas shift (RWGS) reaction are the two pathways for thermocatalytic $CO_2$ reduction on Group VIII metals[2]. Although methanation produces synthetic natural gas, RWGS generates CO, an important component of syngas. Considerable efforts have been devoted to developing catalysts to achieve high selectivity towards either $CH_4$ or CO[3–9]. However, for designing a selective catalyst, it is very important to first have a fundamental understanding of the site requirements, elementary steps and intermediates, which can ultimately lead to the construction of viable mechanisms for both methanation and RWGS. Although intricate interplay between various surface species at different catalyst components that determine product selectivity has been recognized, controversies still exist regarding the detailed mechanism and the roles of surface species[10–15]. Some issues may originate from the different interrogation methods used; for example, some prior conclusions were based on kinetic and spectroscopic information acquired under transient conditions[12]. Under transient conditions, the perturbation of the chemical environment around the adsorbates and catalyst surface causes characteristically divergent behaviors from steady state.

Steady-state isotopic transient kinetic analysis (SSITKA) has evolved as one of the most powerful techniques allowing measurements at steady state to determine the mean surface lifetimes and abundances of intermediates leading to products[16, 17]. However, SSITKA itself cannot identify the chemical nature of surface species, a task that can be accomplished by *operando* spectroscopic measurements, e.g., Fourier transform infrared spectroscopy (FTIR). Correlating the reaction kinetics with the transformations of spectroscopically observable surface species, both simultaneously measured under steady-state reaction conditions, is vital for the complete elucidation of the complex mechanistic framework[18–21]. Pd-based catalysts are able to catalyze both $CO_2$ methanation and RWGS[22, 23]. Our previous work on $Pd/Al_2O_3$ bifunctional catalysts has proposed the plausible pathways for both $CO_2$ methanation and RWGS[24]. However, the factors that govern product selectivity (to $CH_4$/CO) under steady-state $CO_2$ reduction conditions are still not clear.

Here we show that $CH_4$ and CO selectivities are governed by the balance of the hydrogenation kinetics between adsorbed formates and carbonyls over $Pd/Al_2O_3$ catalysts, which was demonstrated by a combined *operando* transmission FTIR spectroscopy/SSITKA investigation. Using this knowledge, we show that tailor-made catalysts can be prepared to achieve high selectivity to either of the two desired products.

## Results

**Steady-state isotopic transient kinetic analysis**. Figure 1a, b show normalized mass spectrometry (MS) responses of gases in the effluent after the feed gas was switched at 0 s from $^{12}CO_2/H_2/Ar$ to $^{13}CO_2/H_2$ at 533 K. The fast disappearance of Ar gas in <4 s indicates a short gas hold-up time for the system. The disappearance of $^{12}CO_2$ was almost as fast as Ar, indicating weak interaction between $^{12}CO_2$ and the catalyst and the reactor walls. In the meantime, the concentration of $^{13}CO_2$ signal increased accordingly, with the concentration and the conversion (2.5%) of carbon dioxide ($^{12}CO_2 + {}^{13}CO_2$) constant during the switch. The decaying signals of $^{12}CH_4$ and $^{12}CO$ and the rising signals of $^{13}CH_4$ and $^{13}CO$ crossed at $y = 0.5$, indicating constant rates for methane and carbon monoxide formation regardless of isotopic substitution. These symmetrical responses indicate that the steady state of the catalyst surface was not perturbed during the switch. The concentrations of products $^{12}CH_4$ and $^{12}CO$ decreased more slowly than that of $^{12}CO_2$ and disappeared at ~600 s. This indicates large mean residence times for C-containing surface intermediates leading to the products, and that intermediates which equilibrate with $CO_2$ are not involved in the rate-determining steps for $CO_2$ methanation and RWGS.

Figure 1c shows the corresponding *operando* FTIR contour plot. Before the switch, the absorption band between 2,300 and 2,400 $cm^{-1}$ (red range) is attributed to gaseous $^{12}CO_2$. The spectral range between 1,800 and 2,100 $cm^{-1}$ (blue and green range) is assigned to chemisorbed carbonyls ($^{*12}CO$) on the surface of Pd metal particles[22]. The absorption bands around 1,400 (yellow range) and 1,600 $cm^{-1}$ (red range) arise from adsorbed formates ($H^{12}COO^*$) on the surface of the $Al_2O_3$

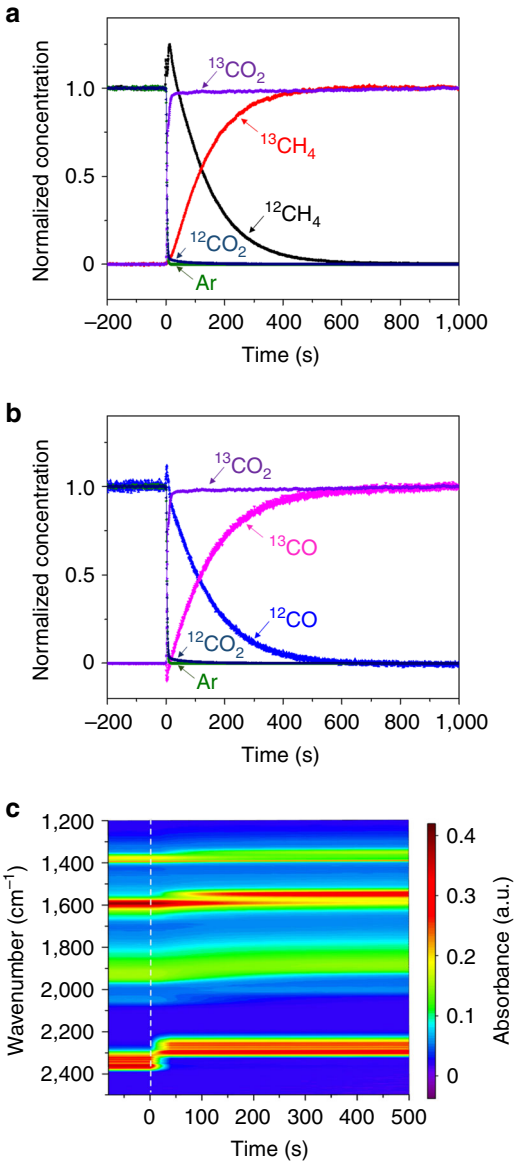


**Fig. 1** The responses of reactants, products and surface intermediates after the steady-state isotopic switch. **a**, **b** Normalized mass spectrometry signals of gases in the effluent and **c** FTIR contour plot collected as a function of time. The feed gas was switched at 0 s from $^{12}CO_2/H_2/Ar$ to $^{13}CO_2/H_2$ over 5% $Pd/Al_2O_3$ at 533 K. Ar gas was used as an inert tracer

support[22]. After the switch, the bands due to $^{12}CO_2$ quickly disappeared and a new band developed at lower wavenumbers (red range between 2,200 and 2,300 $cm^{-1}$) attributable to $^{13}CO_2$, consistent with their rapid responses in MS. The IR signal decay of surface species might be slightly affected by the location of IR beam on the sample wafer[25]. However, the shift of the IR features of $^{12}CO^*$ and $H^{12}COO^*$ to those of $^{13}CO^*$ and $H^{13}COO^*$ at lower wavenumbers were much slower compared with the shift of $^{12}CO_2$ to $^{13}CO_2$ bands. This observation suggests that neither $H^{12}COO^*$ nor $^{12}CO^*$ undergoes reverse reactions to form $^{12}CO_2$. The disappearance trends of the IR signatures of $H^{12}COO^*$ and $^{12}CO^*$ are similar to those of the MS signals of $^{12}CH_4$ and $^{12}CO$ products, suggesting that both $H^{12}COO^*$ and $^{12}CO^*$ are reactive intermediates rather than spectators and, the rate-determining steps for $CH_4$ and CO formation are related to CO* and HCOO*. It is noteworthy that no other species (e.g., bicarbonate) were observed under steady-state reaction conditions and no carbon deposition was identified in our previous study on $Pd/Al_2O_3$ during $CO_2$ reduction[24]. Therefore, CO* and HCOO* are the two most abundant surface species and will be the focus of the following discussion.

To gain insight into the interaction between *CO and Pd on the 5% $Pd/Al_2O_3$, room temperature $^{12}CO$ adsorption followed by temperature-programed $^{*12}CO$ desorption were studied by FTIR (Supplementary Fig. 1). At room temperature $^{*12}CO$ on Pd showed IR features at 2,098, 2,052, 1,960 and 1,928 $cm^{-1}$. When the temperature was raised to 533 K, $^{*12}CO$ with features at 2,098 and 1,960 $cm^{-1}$ desorbed, whereas $^{*12}CO$ with bands at 2,052 and 1,928 $cm^{-1}$ did not desorb but was hydrogenated to $CH_4$ once $H_2$ was introduced. This reveals the existence of two types of adsorption sites on the Pd particles that bind CO weakly ($^{*12}CO_w$) and strongly ($^{*12}CO_s$). The stability of $^*CO_s$ at high temperatures is due to the dissociated *H, which adsorbs near to $^*CO_s$ on the Pd surface and transfers electron density to Pd to strengthen the Pd-CO bond[22, 26]. The FTIR spectrum of $^{*12}CO_s$ is very similar to that of $^{*12}CO$ obtained in $CO_2$ reduction at 533 K, indicating that all $^{*12}CO$ observed under reaction conditions were $^{*12}CO_s$. However, $^{*12}CO_w$ could not be observed during $CO_2$ reduction at $\geq$ 533 K due to its rapid desorption. As we observe no $^{*12}CO_w$ under steady-state reaction conditions, the $^{12}CO$ product generated after the switch was mainly from the conversion of the other abundant species, $H^{12}COO^*$.

Normalized MS responses of $^{12}CH_4$ and $^{12}CO$ with increasing temperature are shown in Supplementary Fig. 2, whereas those for $^{13}CH_4$ and $^{13}CO$ are not displayed. The faster decay in both $^{12}CH_4$ and $^{12}CO$ signals at higher temperatures indicates the higher reactivities of intermediates. In contrast, the decay curves of $^{12}CO_2$ and Ar did not change with temperature, further indicating that any elementary step that directly involves $CO_2$ is not the rate-limiting step for the formation of $CH_4$ and CO. The real mean surface residence times $\overline{\tau}_0$ (Supplementary Fig. 3) of intermediates leading to $^{12}CH_4$ and $^{12}CO$ (denoted as ICH and ICO) together with the $\overline{\tau}_0$-derived activation energies $E$ for $^{12}CH_4$ and $^{12}CO$ formation (Supplementary Fig. 4) are summarized in Table 1. The $\overline{\tau}_{0\_ICH}$ at 533 K was 134 s and gradually decreases with increasing temperature, reaching 41 s at 573 K. Similarly, the $\overline{\tau}_{0\_ICO}$ decreased from 107 to 55 s with increasing temperature from 533 to 573 K. The activation energies are 75 and 53 kJ $mol^{-1}$ for the formation of $CH_4$ and CO, respectively, in line with the values we obtained previously in a plug-flow reactor[24]. Series of corresponding *operando* FTIR spectra of *CO and HCOO* collected at 533–573 K are shown in Supplementary Figs. 5, 6, respectively. The shift of IR bands representing $^{*12}CO_s$ and $H^{12}COO^*$ to those representing $^{*13}CO_s$ and $H^{13}COO^*$ became faster with increasing temperature, but still remained much slower than the shift of the IR band of $^{12}CO_2$ to that of $^{13}CO_2$. The decay trends of $^{*12}CO_s$ and $H^{12}COO^*$ FTIR intensity with increasing temperature was very similar to the decay trends of MS signals of $^{12}CH_4$ and $^{12}CO$ products (Supplementary Fig. 2), further indicating that HCOO* and CO* are related to the rate determining steps for CO and $CH_4$ formation. In addition, the disappearances of $^{*12}CO_s$ and $H^{12}COO^*$ follow an apparent first-order kinetics. The activation energies based on the Arrhenius plots of the two first-order rate constants (Supplementary Figs. 5, 6) are listed in Table 1. The activation energy for the conversion of $^{*12}CO_s$ was 73 kJ $mol^{-1}$, an identical value to that determined for $^{12}CH_4$ formation from the MS data. This result suggests that the rate-determining step along the $CH_4$ formation path is the conversion of $^*CO_s$. The activation energy of $H^{12}COO^*$ conversion was 52 kJ $mol^{-1}$, very similar to the 53 kJ $mol^{-1}$ determined for the $^{12}CO$ formation by MS, indicating that the conversion of HCOO* is the rate-determining step for CO formation.

**Table 1 Real mean surface residence times for ICH ($\overline{\tau}_{0\_ICH}$) and ICO ($\overline{\tau}_{0\_ICO}$), and activation energies for $CH_4$ ($E_{CH4}$) and CO ($E_{CO}$) formation and adsorbed *COs ($E$*COs) and HCOO* ($E_{HCOO*}$) conversions in $CO_2$ reduction at 533–573 K**

| Temp. (K) | $\overline{\tau}_{0\_ICH}$ (s) | $\overline{\tau}_{0\_ICO}$ (s) | $E_{CH4}$ (kJ $mol^{-1}$) | $E_{CO}$ (kJ $mol^{-1}$) | $E_{*COs}$ (kJ $mol^{-1}$) | $E_{HCOO*}$ (kJ $mol^{-1}$) |
|---|---|---|---|---|---|---|
| 533 | 134 | 107 | | | | |
| 543 | 92 | 85 | 75 | 53 | 73 | 52 |
| 563 | 49 | 57 | | | | |
| 573 | 41 | 55 | | | | |

Uncertainties in activation energies are ±2 kJ $mol^{-1}$

**Abundance of surface intermediates**. Figure 2 shows the surface abundance ($\overline{N}$) of ICH and ICO from SSITKA at 533–573 K. The $\overline{N}_{ICO}$ was 1.86 µmol at 533 K, and decreased to 1.01 µmol as the temperature was increased to 573 K. As demonstrated above, $^{12}CO$ was produced from the existing $H^{12}COO^*$. Thus, the amount of $H^{12}COO^*$ that was converted to $^{12}CO$ was less at higher temperatures than at lower temperatures. In contrast, the $\overline{N}_{ICH}$ increased from 1.95 µmol at 533 K to 2.37 µmol at 573 K. This increase could be interpreted as being caused by an increased concentration of $^{*12}CO_s$ at higher temperatures. However, this is not the case, as no difference in intensity of $^{*12}CO_s$ was observed as the temperature was increased from 533 to 573 K (Supplementary Fig. 7). The constant intensity of $^{*12}CO_s$ implies that the amount of $^{12}CH_4$ produced from $^{*12}CO_s$, which have already existed at the moment of the switch, should be the same at 533–573 K. Therefore, the significant increase in the amount of $^{12}CH_4$ at higher temperatures is attributed to the conversion of the other abundant species, $H^{12}COO^*$. These results suggest that with increasing temperature, for a given amount of surface HCOO* at steady state, a progressively larger portion enters the $CO_2$ methanation pathway, while a smaller portion enters the RWGS pathway (Fig. 2b). This explains the decreased $\overline{N}_{ICO}$ at higher temperature. This also agrees well with the above SSITKA results, which show that the $\overline{\tau}_{0\_ICH}$ became shorter than $\overline{\tau}_{0\_ICO}$ with increasing temperature. Therefore, formates prefer to enter the faster pathway to form $CH_4$ rather than enter the slower pathway to form CO at higher temperature. Similarly, Goodwin et al. discussed a case where two products share an intermediate: if $\overline{\tau}_1 > \overline{\tau}_2$, then it must be that $\overline{N}_1 < \overline{N}_2$, because more of this intermediate will form product 2 than product 1 due to the faster

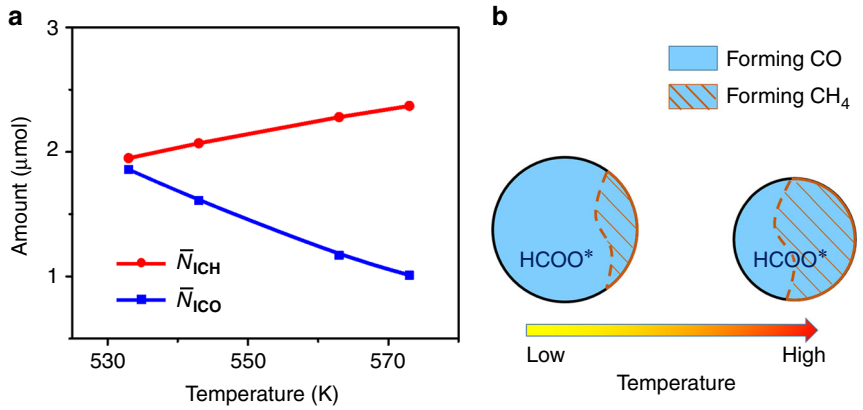


**Fig. 2** The distribution of surface intermediates in the pathways under steady state. **a** The amount of surface intermediates leading to $^{12}CH_4$ ($\bar{N}_{ICH}$) and $^{12}CO$ ($\bar{N}_{ICO}$) on the catalyst (41 mg) during $CO_2$ reduction at 533–573 K. **b** Schematic representation of the proportion of surface coverage of HCOO* that is eventually converted to $CH_4$ and CO with increasing temperature concluded from **a**

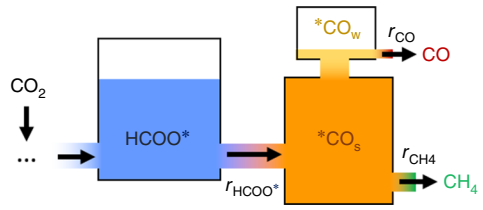


**Fig. 3** Factors governing the selectivities in $CO_2$ reduction. Scheme for the pathways from formate to products in $CO_2$ methanation and RWGS over $Pd/Al_2O_3$ catalysts. The filled pool of $^*CO_s$ and the unfilled pool of HCOO* are supported by the unchanged coverage of $^{*12}CO_s$ and the changed coverage of $H^{12}COO^*$ at 533–573 K (Supplementary Fig. 7)

formation of product 2 (smaller $\bar{\tau}_2$)[27]. Therefore, the temperature effect on these parameters, $\bar{\tau}_{0\_ICH}$, $\bar{\tau}_{0\_ICO}$, $\bar{N}_{ICH}$ and $\bar{N}_{ICO}$, further demonstrates that HCOO* is the intermediate shared by the processes of both $CO_2$ methanation and RWGS.

## Discussion

Based on above results and SSITKA theory[16, 17], a scheme relating HCOO*, $^*CO_s$ and $^*CO_w$ species in $CO_2$ reduction is proposed in Fig. 3. The reduction of formate produces *CO that first occupies strong adsorption sites on the Pd particles. Once the strong adsorption sites of Pd particles are saturated (the pool of $^*CO_s$ is completely filled), the excess *CO can only occupy the weak adsorption sites of Pd particles to form $^*CO_w$. The $^*CO_s$ will be further hydrogenated to $CH_4$ while the $^*CO_w$ will desorb.

The scheme shows that the rate of CO formation ($r_{CO}$) is determined and equal to the rate of HCOO* conversion ($r_{HCOO^*}$) subtracted by the rate of $CH_4$ formation ($r_{CH4}$):

$$r_{CO} = r_{HCOO^*} - r_{CH4} \quad (1)$$

The rate of $CH_4$ formation is equal to the rate of $^*CO_s$ conversion ($r_{^*COs}$, the rate-determining step for $CH_4$ formation), which is proportional to the concentration of $^*CO_s$. The completely filled pool of $^*CO_s$ in the 533–573 K temperature range suggests that $r_{^*COs}$ has reached its maximum, $r_{^*COs\_max}$, at each given temperature between 533–573 K. Therefore, it is the balance between the rate of HCOO* reduction to *CO ($r_{HCOO^*}$) and the maximum rate of $^*CO_s$ conversion ($r_{^*COs\_max}$) that determines whether CO is observed in the gas phase or not. If $r_{HCOO^*} > r_{^*COs\_max}$, both $CH_4$ and CO will be observed (e.g., the case in Fig. 3). If, however, $r_{HCOO^*} \le r_{^*COs\_max}$, which means that all the *CO produced from HCOO* are not sufficient to saturate all strong adsorption sites on the Pd metal for $CH_4$ formation (i.e., the pool of $^*CO_s$ in Fig. 3 is not full or just full), then all *CO will be $^*CO_s$ and will be further hydrogenated to $CH_4$. In this case, $CO_2$ reduction will only be methanation and the rate of $CH_4$ formation $r_{CH4}$ ($r_{^*COs}$) will not reach its maximum$r_{^*COs_max}$.

As the conversions of both HCOO* and $^*CO_s$ require the presence of *H (absorbed hydrogen) involved[24], $r_{CH4}$ ($r_{^*COs\_max}$) is determined by the concentrations of $^*CO_s$ ([$^*CO_s$]) and *H ([*H]), as well as the rate constant of $^*CO_s$ conversion ($k_1$):

$$r_{CH4} = r^*_{COs\_max} = k_1[^*CO_s][^*H] \quad (2)$$

and $r_{HCOO^*}$ is determined by the concentration of HCOO* ([HCOO*]) and *H ([*H]), and rate constant of HCOO* reduction ($k_2$):

$$r_{HCOO^*} = k_2[HCOO^*][^*H], \quad (3)$$

so

$$r_{CO} = r_{HCOO^*} - r_{CH4} = r_{HCOO^*} - r^*_{COs\_max} = k_2[HCOO^*][^*H] - k_1[^*CO_s][^*H] \quad (4)$$

It is known that $^*CO_s$ and HCOO* do not share and compete for active sites, as they are located on Pd metal and $Al_2O_3$ support, respectively[22]. Therefore, [$^*CO_s$] and [HCOO*] can be independently changed to tune the rate of CO formation, $r_{CO}$, as well as the reaction product distribution.

In the case of a completely filled pool of $^*CO_s$ (e.g., the case in Fig. 3), if aiming at a higher $CH_4$ selectivity, [$^*CO_s$] should be increased or [HCOO*] should be decreased. One method, e.g., is to add more metal sites onto the $Al_2O_3$ support. The increased metal loading will not only result in an increased number of metal sites for forming $^*CO_s$ but also lead to a decreased number of support sites that can accommodate HCOO*. It means that the capacity of $^*CO_s$ pool (Fig. 3) is enlarged, meanwhile that of HCOO* is decreased. This, consequently, may lead to a situation where the result of Eq. (4) decreases even to 0, showing less or complete absence of CO in the gas phase. This hypothesis was tested on $Pd/Al_2O_3$ catalysts with different Pd loadings but similar Pd particle size distributions (Fig. 4), which minimized the potential effects of metal particle size on $k_1$ and $k_2$ influencing $r_{^*COs\_max}$ and $r_{HCOO^*}$. If the scheme and hypothesis are correct, $Pd/Al_2O_3$ catalysts with higher Pd loadings should exhibit higher $CH_4$ selectivity than those with lower Pd loadings. Furthermore,

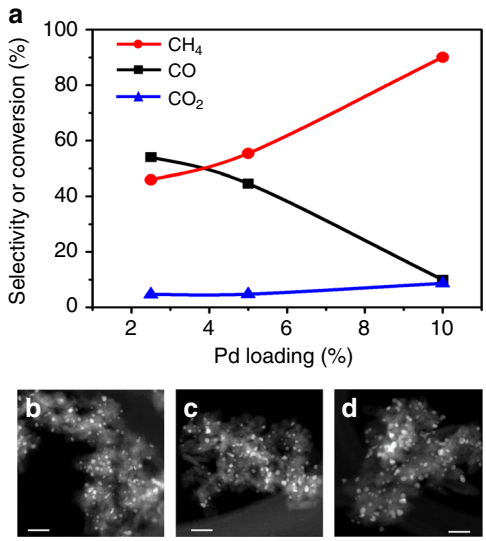


**Fig. 4** Controlled selectivities in $CO_2$ reduction by tailor-made catalysts through mechanistic understanding. **a** $CH_4$ and CO selectivities and $CO_2$ conversion as a function of Pd loading at 573 K. **b**–**d** STEM images of 2.5, 5 and 10% $Pd/Al_2O_3$. STEM scale bars represent 20 nm. (Particle size distributions and temperature-programed $^{*12}CO$ desorption for the catalysts are displayed in Supplementary Fig. 8)

this is exactly what the reactivity data of Fig. 4 shows: $CH_4$ selectivity increased from 45 to 90% as the Pd loading was increased from 2.5 to 10% (Fig. 4). Previous studies on $Ru/Al_2O_3$ and $Ni/SiO_2$ catalysts have also shown that $CH_4$ selectivity in $CO_2$ reduction reaction increased with the metal loading[12, 28, 29], consistent with the findings reported in this work.

In the case of an incompletely filled pool of $^*CO_s$, when $CH_4$ selectivity is always 100%, if one aims at a higher $CH_4$ formation rate, $[^*CO_s]$ needs to be increased. For instance, Karelovic et al.[30] reported that the rate of $CO_2$ methanation over $Rh/Al_2O_3$ was greatly increased by adding $Pd/Al_2O_3$, which has no activity towards $CO_2$ methanation at 473 K. They attributed the synergistic effect to the supply of dissociated $H^*$ from $Rh/Al_2O_3$ to $Pd/Al_2O_3$. It is noteworthy that although $CO_2$ methanation cannot proceed on $Pd/Al_2O_3$ at 473 K, this temperature is high enough for RWGS reaction to occur producing CO[22, 31]. We propose that CO or $^*CO$ produced by/on $Pd/Al_2O_3$ could diffuse onto the Rh domains, increasing the concentration of $^*CO_s$ on Rh. The total amount of $^*CO_s$ produced by both $Pd/Al_2O_3$ and $Rh/Al_2O_3$ is still not enough to saturate all the active Rh sites for $CH_4$ formation (to fill up the $^*CO_s$ pool of Rh, Fig. 3). Therefore, the $CH_4$ selectivity remained ~100% but the methanation rate was higher on the $Pd/Al_2O_3$-$Rh/Al_2O_3$ mixture than on $Rh/Al_2O_3$ alone. The role of the $Pd/Al_2O_3$ component was to provide extra CO ($^*CO$) to the empty sites of Rh. The synergistic effect at lower catalyst temperature (423 K) was found to be negligible. Our study showed that RWGS cannot occur over $Pd/Al_2O_3$ at 423 K[31], so the added $Pd/Al_2O_3$ cannot supply additional CO to $Rh/Al_2O_3$ catalyst for the further $^*CO$ hydrogenation to $CH_4$ on $Rh/Al_2O_3$. Therefore, the above analysis of their results show that for an incompletely filled pool of $^*CO_s$ with 100% $CH_4$ selectivity ($r_{HCOO^*} \leq r_{^*COs\_max}$) on a catalyst, adding a component (promoter) which can produce CO ($^*CO$) is a strategy for increasing the rate of $CO_2$ methanation.

In conclusion, $CO_2$ methanation and RWGS are not two parallel reactions during the $CO_2$ reduction over $Pd/Al_2O_3$ catalysts. Instead, they share the initial steps and intermediates from bicarbonates to formates until after formate decomposition. The rate of formate decomposition to $CO^*$ is larger than the rate of $^*CO$ hydrogenation to $CH_4$ and the excess $CO^*$ desorbs. The rate-determining step for $CO_2$ reduction and for RWGS is the conversion of $HCOO^*$, whereas that for $CH_4$ formation is the hydrogenation of $^*CO$. The balance of the hydrogenation kinetics between $HCOO^*$ and $^*CO$ governs the selectivities to $CH_4$ and CO. Given that $^*CO$ and $HCOO^*$ are mainly on metal (Pd) and support ($Al_2O_3$), respectively, the balance could be tuned to achieve the desired $CH_4$ and CO selectivities by optimizing the loading of the metal and the surface area of the support. This work has important implications for other bifunctional systems where the balance between different catalytic functions determines the rates and product distribution.

## Methods

**Catalyst synthesis and SSITKA experiments**. The $Pd/Al_2O_3$ catalysts were prepared on a γ-$Al_2O_3$ powder (Sasol, Puralox SBA-200) by the incipient wetness method using $Pd(NH_3)_4(NO_3)_2$ as the precursor. After impregnation, the samples were dried at 373 K for 24 h and then calcined at 773 K for 2 h in air (flow rate = 60 mL $min^{-1}$) and followed by reduction at 773 K for 1 h in 10% $H_2$/He (flow rate = 60 mL $min^{-1}$) to obtain the $Pd/Al_2O_3$ catalysts[31]. Forty-one milligrams of 5 wt% $Pd/Al_2O_3$ was pressed onto a tungsten mesh and loaded into a home-made *operando* transmission IR cell[32]. The cell has a very small internal dead volume (~0.2 $cm^3$ after the catalyst loading), resulting in a short gas hold-up time. This renders the system suitable for obtaining accurate kinetic information about intermediates and products during the SSITKA experiments. Before experiments, the catalyst was pretreated by calcination at 673 K for 1 h under air with a flow rate of 10 mL $min^{-1}$, followed by reduction at 673 K for 1 h under 20% $H_2$ in He with a flow rate of 10 mL $min^{-1}$. The reactant gas mixture was composed of 4 mL $min^{-1}$ $H_2$, 1 mL $min^{-1}$ $^{12}CO_2$ or $^{13}CO_2$, 1 mL $min^{-1}$ Ar and He as the diluent with a total gas flow of 10 mL $min^{-1}$ at atmospheric pressure. Ar gas was used as an inert tracer to correct for gas hold-up of the system and for gas re-adsorption. After the reaction reached steady state at the reaction temperature of 533 K, the reactant was switched from $H_2/^{12}CO_2$/Ar to $H_2/^{13}CO_2$. During the switch, the gaseous effluent from the cell and the species on the catalyst surface were monitored by MS and FTIR, respectively. The switch was performed in the temperature range of 533–573 K, where the $CO_2$ conversion was <8%. In order to obtain the real mean surface residence times ($\bar{\tau}_0$) of intermediates leading to $CH_4$ and CO, space velocity experiments were conducted by varying the total flow rate from 10 to 25 mL $min^{-1}$ at constant partial pressures of $CO_2$ and $H_2$ to exclude gas hold-up and re-adsorption effects.

**Data analysis**. The SSITKA theory has earlier been described extensively[16, 33]. The integration of the normalized step-decay or step-input response always yields the overall mean surface-residence time, $\bar{\tau}$, of all adsorbed surface intermediates, which lead to $CH_4$ and CO products ($\bar{\tau} = \int_0^\infty F(t)dt$). The error <5% caused by gas phase hold-up (~3 s) could be ignored due to the fast decay of standard Ar gas and $CO_2$ gas. The rate constant is simply the reciprocal of average surface residence time for the active surface intermediates ($k = \bar{\tau}^{-1} = \mathrm{TOF}^*\theta^{-1}$). The number of adsorbed species ($\overline{N}_{\mathrm{ICH}}$) and CO ($\overline{N}_{\mathrm{ICO}}$) can be obtained from integration of decay rates ($r$) of $CH_4$ and CO products ($\overline{N} = \int_0^\infty r(t)\mathrm{d}t$). In addition, $\overline{N}$ is usually closely related to the number of active sites on the catalysts for product formation. In this study of $CO_2$ reduction over 41 mg of 5% $Pd/Al_2O_3$, the $\overline{N}_{\mathrm{ICO}}$ completely originates from $H^{12}COO^*$, which was demonstrated to be located on the $Al_2O_3$ support. As not all $H^{12}COO^*$ was converted to $^{12}CO$, the amount of sites for formates on $Al_2O_3$ is estimated to be at least 1.86 μmol, i.e., $\overline{N}_{\mathrm{ICO}}$ obtained at 533 K. For $CH_4$ formation via $^{*12}CO_s$ and a portion of $H^{12}COO^*$, the upper limit of the amount of active Pd sites for $^*CO_s$ (forming $CH_4$) is 1.95 μmol, i.e., $\overline{N}_{\mathrm{ICH}}$ at 533 K. This value accounts for 90% of the surface Pd atoms. The total amount of intermediates ($\overline{N}_{\mathrm{CO}} + \overline{N}_{\mathrm{CH4}}$) on the surface of the catalyst slightly decreased from 3.81 μmol at 533 K to 3.38 μmol at 573 K, which was caused by the decreased amount of $H^{12}COO^*$ on the surface shown in Supplementary Fig. 7.

**Data availability**. The data that support the findings of this study are available from the corresponding author on request.

Received: 15 February 2017 Accepted: 7 July 2017
Published online: 11 September 2017

## References

1. Aresta, M., Dibenedetto, A. & Angelini, A. Catalysis for the valorization of exhaust carbon: from $CO_2$ to chemicals, materials, and fuels. technological use of $CO_2$. *Chem. Rev.* **114**, 1709–1742 (2014).
2. Wang, W., Wang, S. P., Ma, X. B. & Gong, J. L. Recent advances in catalytic hydrogenation of carbon dioxide. *Chem. Soc. Rev.* **40**, 3703–3727 (2011).

3. Graciani, J. et al. Highly active copper-ceria and copper-ceria-titania catalysts for methanol synthesis from $CO_2$. *Science* **345**, 546–550 (2014).
4. Sun, W. et al. Heterogeneous reduction of carbon dioxide by hydride-terminated silicon nanocrystals. *Nat. Commun.* **7**, 12553 (2016).
5. Thampi, K. R., Kiwi, J. & Gratzel, M. Methanation and photo-methanation of carbon-dioxide at room-temperature and atmospheric-pressure. *Nature* **327**, 506–508 (1987).
6. Wang, F. et al. Active site dependent reaction mechanism over $Ru/CeO_2$ catalyst toward $CO_2$ methanation. *J. Am. Chem. Soc.* **138**, 6298–6305 (2016).
7. Sun, F. M., Yan, C. F., Wang, Z. D., Guo, C. Q. & Huang, S. L. Ni/Ce-Zr-O catalyst for high $CO_2$ conversion during reverse water gas shift reaction (RWGS). *Int. J. Hydrogen. Energ.* **40**, 15985–15993 (2015).
8. Yeung, C. M. Y. et al. Engineering Pt in ceria for a maximum metal-support interaction in catalysis. *J. Am. Chem. Soc.* **127**, 18010–18011 (2005).
9. Meng, X. G. et al. Photothermal conversion of $CO_2$ into $CH_4$ with $H_2$ over Group VIII Nanocatalysts: an alternative approach for solar fuel production. *Angew. Chem. Int. Ed.* **53**, 11478–11482 (2014).
10. Roiaz, M. et al. Reverse water-gas shift or sabatier methanation on Ni(110)? Stable surface species at near-ambient pressure. *J. Am. Chem. Soc.* **138**, 4146–4154 (2016).
11. Carrasquillo-Flores, R. et al. Reverse water-gas shift on interfacial sites formed by deposition of oxidized molybdenum moieties onto gold nanoparticles. *J. Am. Chem. Soc.* **137**, 10317–10325 (2015).
12. Wu, H. C. et al. Methanation of $CO_2$ and reverse water gas shift reactions on $Ni/SiO_2$ catalysts: the influence of particle size on selectivity and reaction pathway. *Catal. Sci. Technol.* **5**, 4154–4163 (2015).
13. Matsubu, J. C., Yang, V. N. & Christopher, P. Isolated metal active site concentration and stability control catalytic $CO_2$ reduction selectivity. *J. Am. Chem. Soc.* **137**, 3076–3084 (2015).
14. Kattel, S. et al. $CO_2$ hydrogenation over oxide-supported PtCo catalysts: The role of the oxide support in determining the product selectivity. *Angew. Chem. Int. Ed.* **55**, 7968–7973 (2016).
15. Weatherbee, G. D. & Bartholomew, C. H. Hydrogenation of $CO_2$ on group-VIII metals .4. specific activities and selectivities of silica-supported Co, Fe, and Ru. *J. Catal.* **87**, 352–362 (1984).
16. Shannon, S. L. & Goodwin, J. G. Characterization of catalytic surfaces by isotopic-transient kinetics during steady-state reaction. *Chem. Rev.* **95**, 677–695 (1995).
17. Ledesma, C., Yang, J., Chen, D. & Holmen, A. Recent approaches in mechanistic and kinetic studies of catalytic reactions using SSITKA technique. *ACS Catal* **4**, 4527–4547 (2014).
18. Meunier, F. C. et al. Quantitative analysis of the reactivity of formate species seen by DRIFTS over a $Au/Ce(La)O_2$ water-gas shift catalyst: first unambiguous evidence of the minority role of formates as reaction intermediates. *J. Catal.* **247**, 277–287 (2007).
19. Meunier, F. C. The power of quantitative kinetic studies of adsorbate reactivity by operando FTIR spectroscopy carried out at chemical potential steady-state. *Catal. Today* **155**, 164–171 (2010).
20. Wang, J., Kispersky, V. F., Delgass, W. N. & Ribeiro, F. H. Determination of the Au active site and surface active species via operando transmission FTIR and isotopic transient experiments on 2.3 wt.% $Au/TiO_2$ for the WGS reaction. *J. Catal.* **289**, 171–178 (2012).
21. Hanspal, S., Young, Z. D., Shou, H. & Davis, R. J. Multiproduct steady-state isotopic transient kinetic analysis of the ethanol coupling reaction over hydroxyapatite and magnesia. *ACS Catal* **5**, 1737–1746 (2015).
22. Erdohelyi, A., Pasztor, M. & Solymosi, F. Catalytic-hydrogenation of $CO_2$ over supported palladium. *J. Catal.* **98**, 166–177 (1986).
23. Solymosi, F., Erdohelyi, A. & Lancz, M. Surface interaction between $H_2$ and $CO_2$ over palladium on various supports. *J. Catal.* **95**, 567–577 (1985).
24. Wang, X., Shi, H., Kwak, J. H. & Szanyi, J. Mechanism of $CO_2$ hydrogenation on $Pd/Al_2O_3$ catalysts: kinetics and transient DRIFTS-MS studies. *ACS Catal* **5**, 6337–6349 (2015).
25. Thomas, S. et al. Modelling a reactor cell for operando IR studies: From qualitative to fully quantitative kinetic investigations. *Catal. Today* **283**, 176–184 (2017).
26. Solymosi, F., Erdohelyi, A. & Bansagi, T. Infrared study of the surface interaction between $H_2$ and $CO_2$ over rhodium on various supports. *J. Chem. Soc. Farad. T. 1* **77**, 2645–2657 (1981).
27. McClaine, B. C. & Davis, R. J. Importance of product readsorption during isotopic transient analysis of ammonia synthesis on Ba-promoted Ru/BaX catalyst. *J. Catal* **211**, 379–386 (2002).
28. Wang, X., Hong, Y. C., Shi, H. & Szanyi, J. Kinetic modeling and transient DRIFTS-MS studies of $CO_2$ methanation over $Ru/Al_2O_3$ catalysts. *J. Catal.* **343**, 185–195 (2016).
29. Kwak, J. H., Kovarik, L. & Szanyi, J. $CO_2$ reduction on supported $Ru/Al_2O_3$ catalysts: Cluster size dependence of product selectivity. *ACS Catal* **3**, 2449–2455 (2013).
30. Karelovic, A. & Ruiz, P. Improving the hydrogenation function of Pd/gamma-$Al_2O_3$ catalyst by Rh/gamma-$Al_2O_3$ addition in $CO_2$ methanation at low temperature. *ACS Catal* **3**, 2799–2812 (2013).
31. Kwak, J. H., Kovarik, L. & Szanyi, J. Heterogeneous catalysis on atomically dispersed supported metals: $CO_2$ reduction on multifunctional Pd catalysts. *ACS Catal* **3**, 2094–2100 (2013).
32. Yang, Y. et al. Design and operating characteristics of a transient kinetic analysis catalysis reactor system employing in situ transmission Fourier transform infrared. *Rev. Sci. Instrum.* **77** 094104 (2006).
33. Bertole, C. J., Mims, C. A. & Kiss, G. Support and rhenium effects on the intrinsic site activity and methane selectivity of cobalt Fischer-Tropsch catalysts. *J. Catal.* **221**, 191–203 (2004).


## Acknowledgements

We gratefully acknowledge the financial support of this work by the US Department of Energy (DOE), Office of Science, Office of Basic Energy Sciences, Chemical Sciences, Geosciences and Biosciences Division.

## Author contributions

X.W. designed and built up the SSITKA/*Operando*-FTIR/MS/GC system and performed all the experiments, analyzed the data and wrote the paper. H.S. revised the paper. J.S. managed the project and revised the paper.

## Additional information

**Supplementary Information** accompanies this paper at doi:10.1038/s41467-017-00558-9.

**Competing interests:** The authors declare no competing financial interests.

**Reprints and permission** information is available online at http://npg.nature.com/reprintsandpermissions/

**Publisher's note:** Springer Nature remains neutral with regard to jurisdictional claims in published maps and institutional affiliations.